Predicting bacterial interaction outcomes from monoculture growth and supernatant assays

Désirée A. Schmitz[a], Tobias Wechsler[a], Ingrid Mignot[a] & Rolf Kümmerli [a]

[a] Department of Quantitative Biomedicine, University of Zurich, Zurich, Switzerland

How to derive principles of community dynamics and stability is a central question in microbial ecology. To answer this, bottom-up experimental approaches, in which a small number of bacterial species are mixed, have become popular. However, experimental setups are typically limited because species are difficult to distinguish in mixed cultures and co-culture experiments are labor-intensive. Here, we use a community of four bacterial species to show that information from monoculture growth and inhibitory effects caused by secreted compounds can be combined to reliably predict pairwise species interactions in co-cultures. Specifically, integrative parameters from growth curves allow to build a competitive rank order, which is then adjusted using inhibitory compound effects from supernatant assays. While our procedure worked for two media examined, we observed differences in species rank orders between media. We further used computer simulations, parameterized with our empirical data, to show that higher-order species interactions largely follow the dynamics predicted from pairwise interactions with one important exception. The impact of inhibitory compounds was reduced in higher-order communities because these compounds are spread across multiple species, thereby diluting their effects. Altogether, our results lead to the formulation of three simple rules of how monoculture growth and supernatant assay data can be combined to establish competitive species rank orders in bacterial communities.

bacterial interactions | competitiveness | community dynamics | agent-based model

Correspondence to: *desiree.schmitz@uzh.ch or rolf.kuemmerli@uzh.ch*

Introduction

Microbial communities are diverse in composition and function (1,2). Top-down approaches based on 16s rRNA and shot-gun sequencing are commonly used to describe community diversity and functional capacities, respectively. However, much less is known about the microbial interactions occurring in these communities. This is why bottom-up approaches have become popular, where a set of defined bacterial species and strains are mixed, and their interactions are studied under experimental conditions (3–9). The power of simple communities is that they are tractable and allow for experimental manipulation so that the effect of specific factors on community properties can be examined. There is a plethora of bottom-up studies that shed light on various ecological aspects of species interactions. Key insights from such studies include, for example, that harsh environmental conditions seem to be more conducive for ecological facilitation (3) and for promoting biodiversity and community stability (4). Furthermore, social interactions also appear to be key determinants of community composition and stability, be it through metabolic cross-feeding between species (5,7) or the secretion of competitive and cooperative secondary metabolites (8).

Despite their simplicity, studying experimental communities also comes with several challenges. For example, it is often unclear what the key determinants of interactions are. This is particularly the case for communities for which no a priori knowledge on relevant traits and species characteristics is available. In such cases, there are at least three factors that could determine species interactions and community composition. The first factor is monoculture growth performance, whereby faster growing species are predicted to dominate over slower growing ones (10,11). The second factor involves secreted compounds that could either positively (e.g., amino acids) or negatively (e.g., toxins) affect the growth of other species (4,12–15). The third factor consists of direct cell-to-cell interactions that can only manifest when two species physically meet (16–18). A key challenge is to assess the relative importance of these three factors and how they combine to predict species dominance and community dynamics. Further challenges arise when considering that species interactions might differ across environments (3,4) and that pairwise interactions might not necessarily predict interaction dynamics in larger communities (6).

In our study, we combine experiments and computer simulations on a four-species bacterial consortium to tackle some of these challenges. Our consortium consists of four opportunistic human pathogens (*Burkholderia cenocepacia* [B], *Cronobacter sakazakii* [C], *Klebsiella michiganensis* [K], *Pseudomonas aeruginosa* [P]), and has been established as a model community in one of our earlier studies (19). With this model consortium, we pursue four main aims. First, we ask whether differences in monoculture growth performance and interactions based on stimulatory or inhibitory molecules secreted by bacteria are good predictors of species interactions in pairwise co-culture experiments. Second, we compare whether the observed interaction patterns are consistent across two different nutritional environments: Lysogeny broth (LB) and Graces' insect medium (GIM). While LB is a standard laboratory medium, GIM mimics the environment found in Lepidoptera larvae, a common host model system (20–22). Third, we derive tentative rules to predict pairwise interaction outcomes from monoculture growth and supernatant assays and establish rank orders for competitiveness of the four species. Finally, we parameterize an agent-based model (23,24) with experimental monoculture growth data and growth effects mediated by secreted compounds to examine whether simulated higher-order community interactions recover the competitive rank orders predicted from pairwise co-culture experiments.

Materials and methods

Bacterial strains

For all experiments, we used the following four bacterial species: *Pseudomonas aeruginosa* PAO1 (25), *Burkholderia cenocepacia* K56-2 (26), *Klebsiella michiganensis*, and *Cronobacter sakazakii* (ATCC29004). We had established this consortium of four gram-negative bacterial species in an earlier study (19), in which we were interested in interactions between pathogens with different virulence levels in the larvae of the Greater wax moth *G. mellonella*. While virulence plays no role in the current study, we used the same consortium to be able to compare *in vitro* interactions to those observed *in vivo*.

Monoculture growth assays

All media were purchased from Sigma Aldrich, Switzerland, unless indicated otherwise. All experiments in this study were carried out in lysogeny broth (LB) and Grace's insect medium

(GIM) (Gibco, GIM 1X, supplemented). GIM is a very nutrient-rich medium and consists of 19 different amino acids, 10 different vitamins (e.g., biotin, riboflavin, folic acid), 5 inorganic salts ($CaCl_2$, $MgCl_2$, $MgSO_4$, KCl, NaH_2PO_4-H_2O), and several carbon sources (e.g., fructose, glucose, sucrose). Prior to experiments, each species was taken from a 25% glycerol stock stored at -80° C and grown overnight in 5 mL LB at 37° C and 170 rpm with aeration (Infors HT, Multitron Standard Shaker) until stationary phase. The bacterial cultures were then washed twice with 0.8% NaCl, centrifuging for 5 min at 7,500 rcf (Eppendorf, tabletop centrifuge MiniSpin plus with rotor F-45-12-11). Subsequently, we adjusted the cultures to an optical density at 600 nm (OD_{600}) = 1. Then, each well of a 96-well cell culture plate (Eppendorf, non-treated, flat bottom) was filled with 190 µL medium (LB or GIM) and 10 µL individually diluted cell suspensions to reach a starting number of 10^5 CFU/mL (i.e., $2x10^4$ CFU/well). Plate layouts (i.e., positions of species and replicates on plates) were randomized between experiments. To minimize evaporation, the outer moat space and inter-well spaces of the microplate were filled with 13 mL sterile water. Plates were incubated at 37° C in a microplate reader (Tecan, Infinite MPlex) and OD_{600} was measured every 15 min for 24 h with 60 sec shaking prior to each reading.

We used the Gompertz function to fit growth curves to the obtained OD_{600} trajectories and to extract three different growth parameters: maximum growth rate (μ_{max}), area under the curve (AUC), and the inverse of the time to mid-exponential phase ($1/T_{mid}$). For the latter, we used the inverse of T_{mid} to ensure that low and high values stand for low and high growth, respectively, for all growth parameters.

Supernatant assays

Cells were prepared as for the monoculture growth assays. Washed cell cultures were subsequently inoculated in 10 mL medium within 50 mL Falcon tubes (inoculum size: 10^5 CFU/mL). We had 10 replicates (tubes) per species. Tubes were incubated at 37° C shaken at 170 rpm with aeration (Infors HT, Multitron Standard Shaker). We harvested supernatants when species had reached the stationary phase, which was after 16 hours for C and P, and after 40 h for B and K (Fig. 1). Supernatants from all 10 replicates of a species were pooled and mixed before filter sterilizing them with a 0.2 µm filter (GE Healthcare Life Sciences, Whatman filter) and aliquoting and storing them in 2 mL Eppendorf tubes at -20° C.

For the actual supernatant assays, we prepared cells and distributed them on microplates as described for the monoculture growth assay. The cells were then exposed to three different media: (a) 30% supernatant from another species + 70% fresh medium (LB or GIM), (b) 30% NaCl (0.8% solution) + 70% fresh medium, and (c) 100% fresh medium. Plates were incubated at 37° C in a microplate reader (Tecan, Infinite MPlex) and OD_{600} was measured every 15 min for 24 h with 60 sec shaking prior to each reading. As above, we fitted Gompertz functions to the growth trajectories and extracted μ_{max}, AUC, and $1/T_{mid}$. We then expressed the growth in supernatant relative to the two control treatments, (a)/(b) and (a)/(c). We define growth inhibition if (a)/(b) < 1, and growth stimulation if (a)/(c) > 1.

To obtain a comparable species ranking across assays, we calculated an integrative supernatant score. Specifically, we summed up all the relative growth values (a)/(b) that the supernatant of one species has on the other three species. The four values (one per species) were then centered around 0 and scaled between -1 and +1. Negative and positive values stand for stimulatory and inhibitory supernatant effects, respectively, and are indicative of a species' competitiveness.

Co-culture experiments

Overnight cultures were washed and OD_{600} adjusted as described for the monoculture growth assays. Next, bacterial species were diluted individually to reach similar cell numbers. To obtain 10^5 CFU/mL per well (i.e., $5x10^4$ CFU/mL of one species and $5x10^4$ CFU/mL of the other species), 25 µL from each of the two species' dilutions was added in each well of a 24-well tissue culture plate (Corning, flat bottom with low evaporation lid) filled with 950 µL medium. Well-plates were incubated at 37° C and 170 rpm for 24 h (Infors HT, Multitron Standard Shaker).

After competition, OD_{600} was measured to calculate the appropriate dilution for plating. Calculations were based on previously established calibration curves, relating OD to CFU for each of the four species and averaging the expected CFU between the two species in a mix. Cultures were diluted with 0.8% NaCl, and each replicate was plated in duplicate on LB-agar plates (1.5% agar). We incubated all plates overnight at 37° C and manually counted CFU on the next day. All four species could be distinguished from each other based on their different colony morphologies on plates (see supplementary information of (19)). Since *C. sakazakii* colonies turn yellow after a day at room temperature, we left them on the bench for an additional day. Plates containing *B. cenocepacia* were incubated at 37° C for two days in total because of its slow growth. If one species was much more frequent than the other one, we used selective plating (if available) to ensure that we could assess the abundance of the low-frequency species. For *P. aeruginosa*, we used Pseudomonas isolation agar. For *B. cenocepacia*, we used LB plus gentamicin (30 µg/mL) due to its inherent resistance to this antibiotic. No selective media was available for C, meaning that C could not be counted in co-culture with P below a given detection limit.

The relative fitness values of each focal species were calculated based on Wrightian fitness from Ross-Gillespie et al. (2007) as follows:

$$Relative\ fitness_{Species1} = \frac{(End\ CFU_{Species1} \times Starting\ CFU_{Species2})}{(End\ CFU_{Species2} \times Starting\ CFU_{Species1})}$$

Relative fitness values > 0 and < 0 indicate that the focal species wins or loses in competition with the co-cultured species, respectively. We log-transformed our data to be able to better compare values across species combinations.

We calculated an integrative score to obtain a measure of competitiveness for each species relative to all other species. Given that each relative fitness value can be expressed from the perspective of the winner or the loser (resulting in reciprocal values), we followed a stepwise process to avoid double counting of fitness values. We started with the weakest species and summed up all its relative fitness effects in competition with the three other species. Then we moved to the second (and third) weakest species and repeated the procedure leaving out any fitness effects that were already accounted for before. For the final two species, we only considered their effect on each other.

Agent-based model

We performed agent-based simulations, using our previously developed platform (23,24). Microbial simulations take place on a two-dimensional toroidal surface with connected edges without boundaries. The surface of the torus is 10,000 μm^2 (100 × 100 µm). Bacteria are modeled as discs with an initial radius of 0.5 µm. Bacteria grow through an increase of their radius, according to a growth-function, and divide when reaching the threshold radius of 1 µm. In our simulations, we assumed that resources are not limited. Differences in growth patterns emerge solely based on the differences in growth-rate *g* and interactions between the species. Interactions are modeled via molecules that can be secreted into the environment by bacteria. Molecules can be taken up when they physically overlap with a cell and can either be growth stimulating or inhibitory. In our simulations, we only model inhibitory molecules. Accordingly, the growth of each cell is determined by the function

$$G_t = g \times \left(1 - \left(\frac{\Sigma T_i}{\theta_T}\right)^{\kappa}\right) \times G_0 ,$$

where G_t denotes the increase in radius per time step, g the species-specific growth rate and ΣT the number of accumulated toxins. Toxins decrease growth and lead to cell death when they accumulate beyond the threshold value θ_T. The decrease in growth is further controlled by the latency parameter $\kappa = 2$, which leads to an exponentially increasing (negative) effect on growth, depending on the number of accumulated toxins. If a cell has taken up toxins and divides before the threshold θ_T is reached, the accumulated toxins are shared equally among

the two daughter cells. The factor G_0 denotes the default radius increase per time step (0.5/1,200 μm).

At the beginning of a simulation, bacteria of each strain are randomly placed on the landscape. We started our simulations with 32 cells per species, for pairwise as well as for higher-order communities. Bacteria can disperse on the surface, according to a specific cell diffusion coefficient *D*. The bacteria start to grow and divide according to their life cycle, until the total cell number of 500 is reached. At that point, a chemostat mechanism is activated that keeps the number of cells around the threshold value of 500 by randomly removing cells. The chemostat mechanism allows observing strain dynamics over extended timespans and prevents overgrowth of the surface. We ran all simulations for 30,000 time steps with 20 replicates per parameter and species combination.

To implement differences in growth rates between the four species, we used the scaled differences in $1/T_{mid}$ values from monoculture growth in GIM. To ensure that all species can grow in our simulations, we allocated a value of 0.5 to all species-specific growth rates and an additional value proportional to the $1/T_{mid}$ value of the respective species, according to the formula

$$g = 0.5 + 0.5 \times \frac{Tmid_C}{Tmid}.$$

This resulted in the following species-specific growth rates: C = 1, P = 0.84, K = 0.81 and B = 0.68.

To implement inhibitory effects observed in the supernatant assays in GIM, we allowed strains to produce toxins. We only implemented inhibitory effects that led to a minimum reduction of growth by 20%. This was the case for K inhibiting all other species, and B inhibiting P. To calibrate the strength of toxins, we simulated pairwise competitions between all four species across a range of toxin threshold values θ_T (750 to 4,500, in steps of 250). The aim was to define the minimal toxin potency required to recover the competitive outcomes observed in the co-culture experiments. We found this to be the case when (i) the K-toxin had a potency of 1,750 for C, (ii) the K-toxin had a potency of 2,500 for B and P, and (iii) the B-toxin had a potency of 2,500 for P. Note that low values stand for high toxin potency because fewer toxin molecules are needed to be detrimental for a cell. The pairwise competition outcomes with toxin threshold values of 0, 1,750, 2,125, and 2,500 are shown in Fig. S1. These simulations were carried out under conditions of high cell and molecule diffusion (D = 5 $\mu m^2\ s^{-1}$ and ∂ = 10 $\mu m^2\ s^{-1}$ respectively) to match the experimental setup of a shaken culture.

Following calibration, we modeled higher-order competitions between all four species and all possible three species combinations. For the multispecies interactions, we modeled environments with different diffusion conditions (low: D = 0.0 $\mu m^2\ s^{-1}$, ∂ = 0.1 $\mu m^2\ s^{-1}$, high: D = 5.0 $\mu m^2\ s^{-1}$, ∂ = 10.0 $\mu m^2\ s^{-1}$). For each simulated replicate, we extracted the frequency of each species at each time point, assessed the overall growth performance of each species by calculating the mean species frequency over time, and recorded the per capita toxin uptake per species.

Statistical analyses

All statistical analyses were conducted with R (version 4.1.1) and the interface RStudio (version 2021.09.0+351). We built linear mixed models with experimental date as a random variable (i.e., the same experiments were carried out in independent blocks on different days), for both the monoculture growth and supernatant assays. For monoculture growth, the R function “pairs” from the “emmeans” package was used to automatically adjust the p-values in pairwise comparisons, based on the Tukey method. For the supernatant assays, p-values were adjusted using the FDR method due to multiple pairwise comparisons.

To test whether the relative fitness in any of the pairwise competitions is different from the expected log(1) = 0 value (assuming that both species perform equally well), we used one-sample two-sided Wilcoxon rank tests, since our relative fitness data were not normally distributed.

Results

Monoculture growth parameters as predictors of competitiveness

The performance of a species in monoculture is often taken as a first proxy for its competitiveness in mixed culture, whereby faster growing bacteria are expected to outcompete slower growing bacteria in co-culture (10,11). In a first experiment, we thus grew the four pathogen species in monoculture in our two media (LB and GIM) over 36 hours. From the obtained growth curves, we quantified three different growth parameters: maximum growth rate (μ_{max}), the inverse of the time to mid-exponential phase ($1/T_{mid}$), and the growth integral (area under the curve, AUC).

All species grew better in GIM than in LB, and we observed different growth trajectories between our four bacterial species (Fig. 1A). When focusing on μ_{max}, which is the most commonly used growth parameter, we observed that C and P grew better than B and K, with the differences being larger in GIM than in LB (Fig. 1B). Next, we looked at $1/T_{mid}$, an integrative parameter that is determined by the lag phase, growth rate, and yield (Fig. 1C). While this growth parameter returns C and B as the best and worst grower, respectively, the performance of P is decreased in comparison to its μ_{max} because of its later onset of growth. When considering the growth integral, we found that this parameter dampened the differences between species (Fig. 1D). This is expected as the integral gives more weight to yield (at stationary phase), which is quite similar for all four species.

Our analysis reveals that a species' competitiveness depends on the growth parameter examined. This raises an additional challenge, namely which growth parameter to consider. To address this challenge, we conducted correlation analyses (Fig. S2) and found that all three growth parameters correlate well with each other in GIM (Pearson correlation coefficients, $r = 0.81$ to 0.91). However, this is not the case in LB, where correlations are poor or non-significant ($r = 0.33$ to 0.56). The main reason for the mismatch is P with its high μ_{max} but low $1/T_{mid}$ due to an extended lag-phase, and C with an intermediate μ_{max} but high $1/T_{mid}$ due to a short lag phase (Fig. 1). These considerations explain why the different growth parameters do not necessarily correlate with one another in LB. Since we cannot yet infer which parameter predicts species competitiveness best based on these results alone, we estimated all three growth parameters for both media and show the species rank order for all of them (Fig. 4).

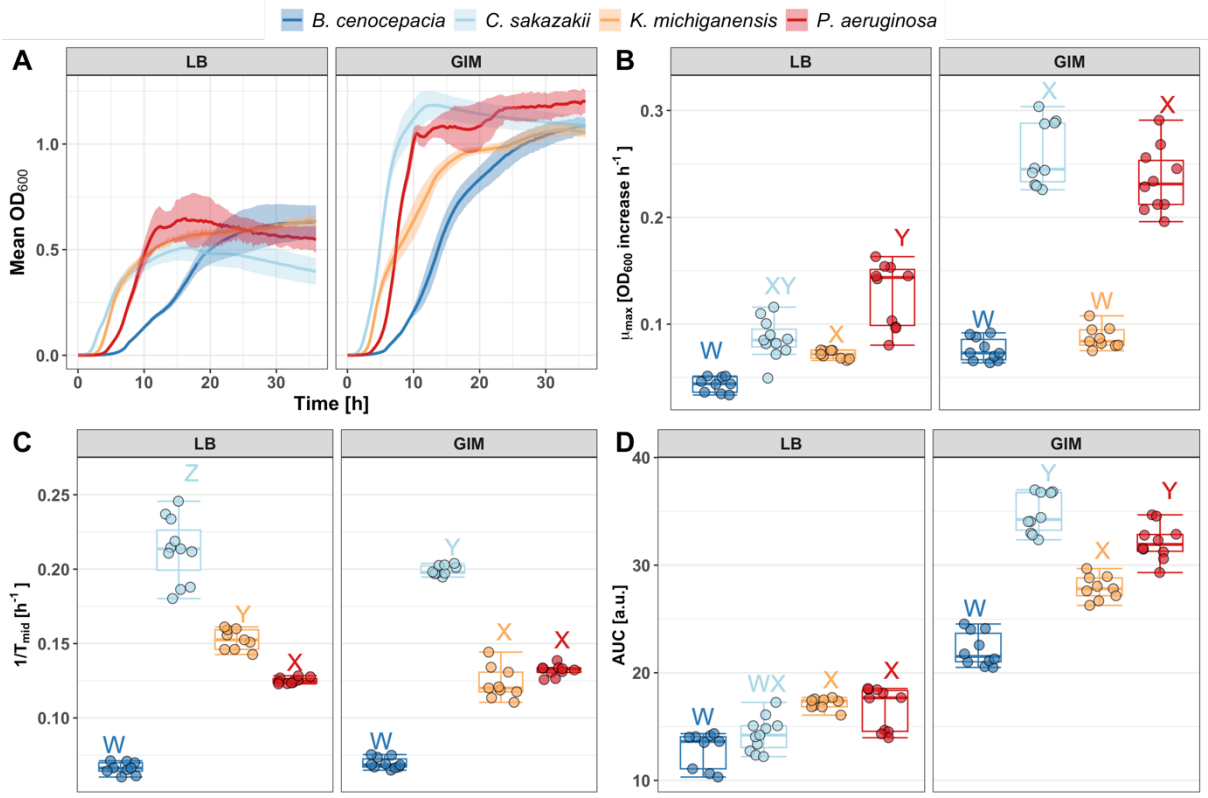

Figure 1. Growth differences of the four bacterial species in two nutrient-rich media: LB medium and Grace's insect medium [GIM]. (A) Growth curves over 36 h in shaken, liquid cultures. Shaded areas depict the standard deviation. Boxplots show the (B) maximum growth rate μ_{max} as OD_{600} increase per hour (C) the inverse of the time to mid-exponential phase [$1/T_{mid}$], and the (D) integral [area under the curve, AUC]. All growth parameters are derived from the growth curves in (A) using the Gompertz curve fit. Letters above boxplots indicate significant growth differences (alpha = 0.05) between bacterial species using linear mixed models with experimental block as random factor. Boxplots show the median (line within the box) with the first and third quartiles. The whiskers cover 1.5x of the interquartile range or extend from the lowest to the highest value if all values fall within the 1.5x interquartile range. Data are from 3 independent experiments, each featuring 3-4 replicates per condition, resulting in a total of 9-10 replicates per condition.

Effect of secreted compounds as predictors of competitiveness

We used supernatant assays to assess whether secreted compounds can predict competitiveness between interacting species. Supernatants contain molecules (e.g., toxins, siderophores, biosurfactants, amino acids) secreted by the producing species that can negatively or positively impact the fitness of the receiving species (4,12–15). To test for such effects, we exposed each of our species to the supernatant (30% supernatant + 70% fresh medium) of all other species and measured the growth effects relative to a control condition (30% NaCl solution [0.8%] + 70% fresh medium). In Figure 2, we present the results with the growth parameter $1/T_{mid}$, while the results for μ_{max} and AUC are shown in Fig. S3 and Fig. S4, respectively.

Similar to the monoculture parameters, we found differences in the supernatant effects between the two media. While there were 5 negative growth effects out of 12 in LB (Fig. 2A) and 6 negative effects out of 12 in GIM (Fig. 2B), 9 out of the 12 interactions changed direction from neutral/positive to negative (or vice versa) between media. For example, the supernatant of K was highly inhibitory for B, C, and P in GIM but not in LB. Overall, we found that supernatants from one species can have

strong inhibitory effects on the growth of another species, but these effects highly vary across media conditions. We also observed positive supernatant effects. Some of these positive effects are indeed caused by the species producing the supernatant (e.g., through nutrient release or the secretion of beneficial compounds such as enzymes) because growth exceeds the level of growth observed in 100% original medium (gray dashed line Fig. 2). In other cases, the positive growth effects are weak and likely explained by leftover nutrients in the supernatant (Figs. S3 and S4).

To obtain an integrative score of how much our four species influence each other's growth indirectly via their supernatant, we summed up all the effects one species has on the others, separately for each of the three growth parameters (i.e., from Fig. 2, S3, and S4). This score yielded species rank orders that differ between growth parameters and media (Fig. 4).

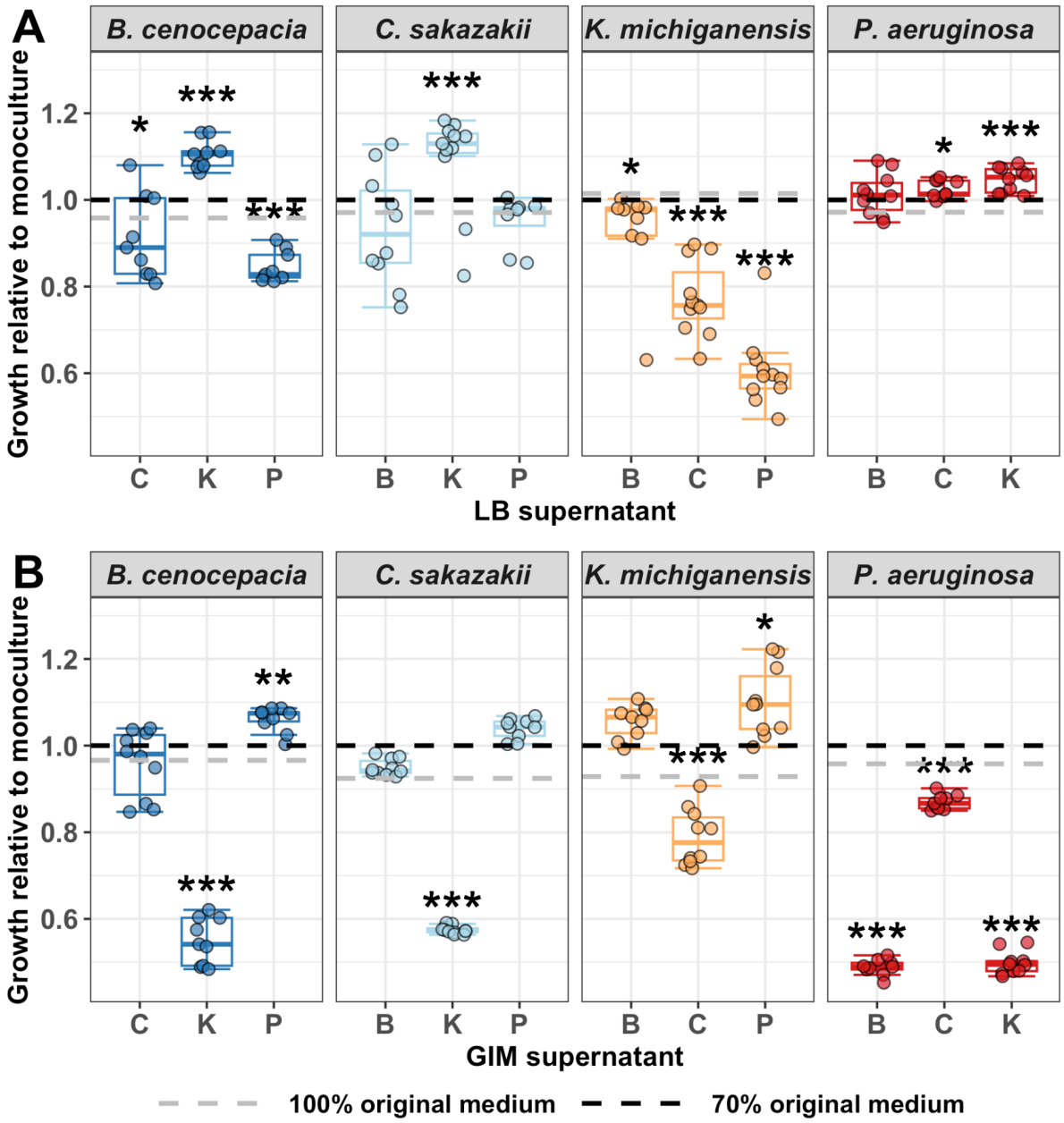

Figure 2. Boxplots show the relative growth of each species in the conditioned medium (30% supernatant + 70% fresh medium) of the other species both in (A) LB and (B) GIM medium,

compared to a control treatment (30% NaCl solution [0.8%] + 70% fresh medium). For this plot, we used $1/T_{mid}$ for growth comparisons. We repeated the same analysis for μ_{max} (Fig. S3) and AUC (Fig. S4). Asterisks depict significant differences (alpha = 0.05) of a species' growth in the particular supernatant compared to its growth in the control medium using a linear mixed model with experimental block as random factor. Boxplots depict the median (line within the box) with the first and third quartiles. The whiskers cover 1.5x of the interquartile range or extend from the lowest to the highest value if all values fall within the 1.5x interquartile range. Data are from 3 independent experiments, each featuring 3-4 replicates per condition, resulting in a total of 9-10 replicates per condition.

Competitiveness in co-culture assays

In a next step, we carried out co-culture experiments in all pairwise combinations of our four bacterial species in both media and determined relative fitness of the competing species after 24 h (Fig. 3). This assay brings together all elements of interactions: differences in the growth performance across species, secreted compounds that affect competitors, and any form of direct interactions, such as beneficial nutrient cross-feeding or competitive interactions via cell-contact dependent secretion systems.

Unlike for the previous competition metrics, we found the results to be much more consistent between LB (Fig. 3A) and GIM (Fig. 3B). The competitive outcomes only changed in 2 out of the 6 comparisons and was pronounced in only one case, in which C lost against P in LB but was the clear winner in GIM. An example of consistency is B that was outcompeted by all competitors in both media. Furthermore, we found that species coexisted in the majority of cases. The only exception occurred in LB, where P seemed to displace B and C in most replicates. As above, we used an integrative score to obtain a measure of competitiveness for each species relative to all other species (Fig. 4) (see Methods for details).

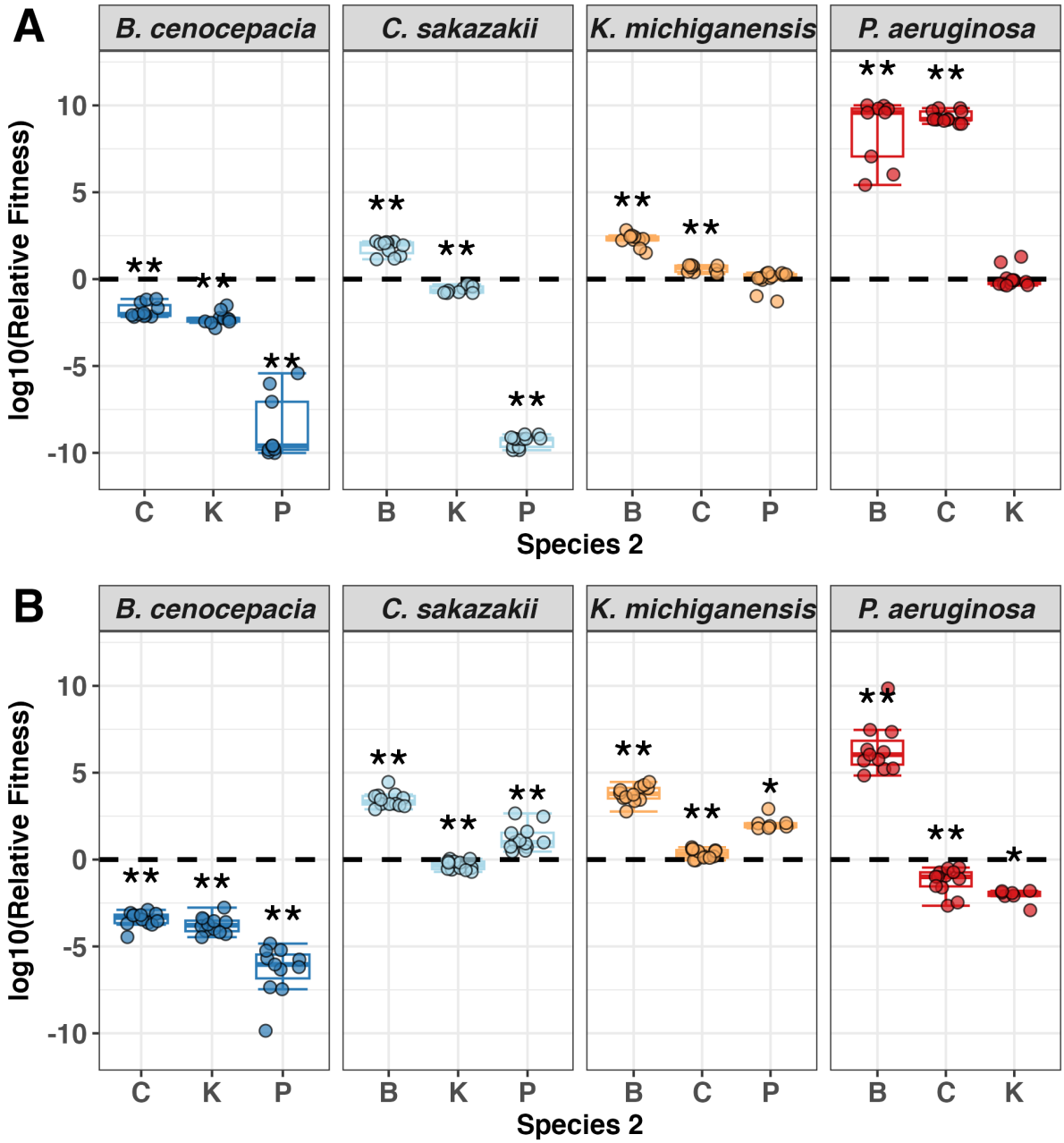

Figure 3. Boxplots show the fitness of the species indicated in the header relative to all other species in co-culture assays in (A) LB and (B) GIM medium. Asterisks depict significant differences (alpha = 0.05) of a species' fitness relative to that of a competitor against the null hypothesis that none of the two species has an advantage (relative fitness = 0, black dashed line) using one-sample two-sided Wilcoxon rank tests. Boxplots show the median (line within the box) with the first and third quartiles. The whiskers cover 1.5x of the interquartile range or extend from the lowest to the highest value if all values fall within the 1.5x interquartile range. Data are from 6 individual experiments with 2 replicates per condition, resulting in a total of 7-12 replicates per condition (note in a few cases sample size was <12 because obtaining countable colonies for both species in co-culture was notoriously hard).

Deriving rules to predict species competitiveness based on monoculture growth and supernatant effects

In this section, we integrate the competitiveness rankings of the four species across all our experiments and ask which metric or combination of metrics is most predictive of the observed outcome in co-culture experiments (Fig. 4).

We start with GIM, as the results are more evident compared to those from LB. In GIM, we find that all monoculture growth parameters positively correlate with one another and return the same species ranking: B < K < P < C. This species ranking matches the outcome of the co-culture experiments well for three species (B < P < C), but not for K. In monoculture, K shows intermediate growth performance but is the most competitive species in co-culture experiments. To explain this apparent mismatch, we consider the results from the supernatant assay (Fig. 2), in which we find that K strongly inhibits all other species (based on $1/T_{mid}$ and AUC). Thus, we can derive two tentative rules to predict competitive outcomes in GIM. Rule 1: take the species rank order based on monoculture growth (B < K < P < C). Rule 2: consider the supernatant effects and adjust the rank order by moving species that strongly inhibit others further up the ranking (B < P < C < K). Interestingly, we find that B (the weakest performer in monoculture) strongly inhibits P in the supernatant assay (Fig. 4), but this inhibition did not lead to a shift in the species rank order in the co-culture experiments. We can thus derive a third tentative rule. Rule 3: inhibitory supernatant effects exerted by slow growing species can be ignored as they do not influence competitiveness in co-culture.

We now turn to LB and realize that the species rank order is different for all three monoculture growth parameters and the corresponding supernatant effects. Nonetheless, we applied our three tentative rules to LB and found a good fit when using the AUC growth parameter. Rule 1: take the monoculture species rank order. For LB (AUC), this is B < C < K < P. Rule 2: consider the supernatant effect and move species that inhibit others further up the ranking (for LB (AUC): first rank: K inhibits B and C / second rank: P inhibits C and K). In this case, the supernatant effects do not induce a major change in the ranking, but a strong clustering into two inferior and two superior species: B ≈ C < P ≈ K. Rule 3: ignore inhibitory supernatant effects of species with poor monoculture growth (for LB (AUC): C inhibits B, but this effect has no consequence for the species rank order and can be ignored). Applying these rules leads to a species ranking for LB co-culture competitions that matches our experimental observations. Based on the LB data, we may further derive that more integrative growth measures – which consider more than one aspect of the growth trajectory ($1/T_{mid}$ and AUC) – might be more informative for competitiveness prediction than growth parameters capturing only a single feature of the monoculture growth dynamics (μ_{max}).

In conclusion, our results indicate that a two-step process, incorporating monoculture growth as the basis and supernatant assay data for fine-tuning, could be sufficient to predict co-culture competitive outcomes in different media based on three simple rules.

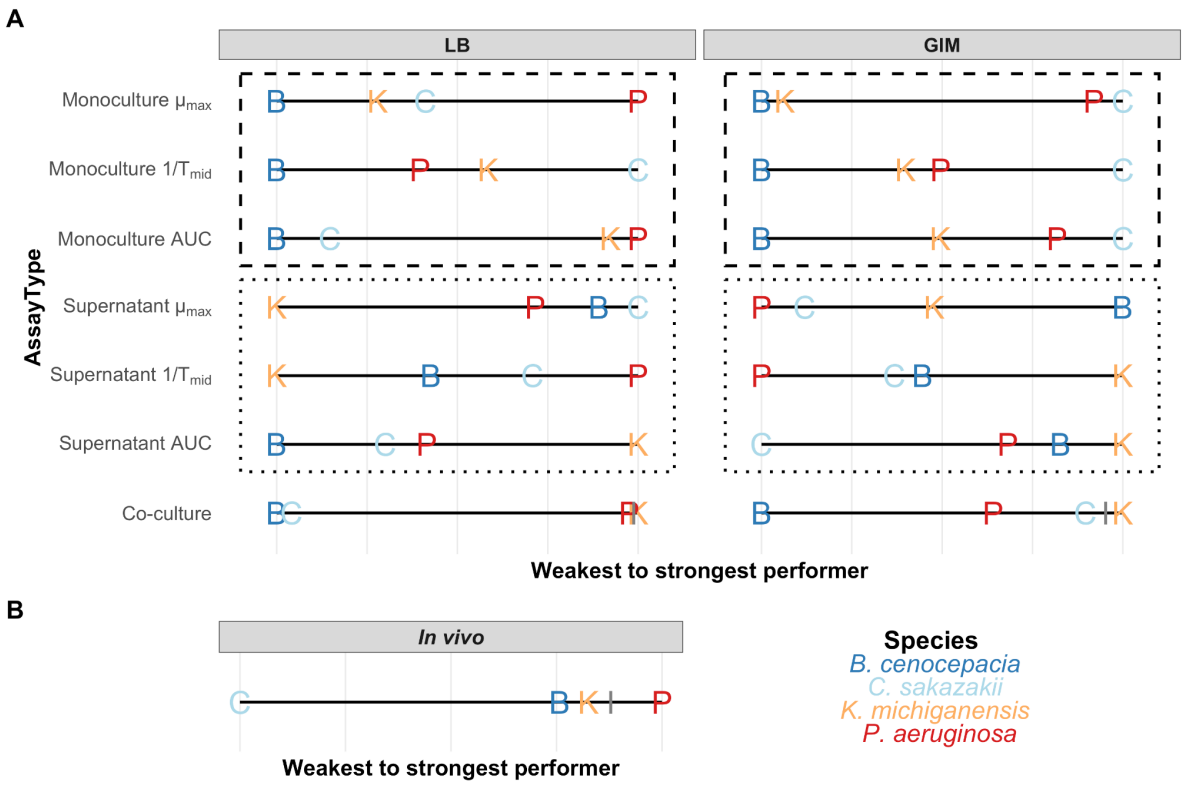

Figure 4. (A) Species rank orders of competitive strength inferred from monoculture growth, the ability of a species to affect the growth of competitors in conditioned medium (supernatant), and co-culture experiments. All *in vitro* experiments were conducted in two different media: LB and GIM. For monoculture growth and supernatant assays, rank orders are shown for maximum growth rate (μ_{max}), the inverse of the time to mid-exponential phase ($1/T_{mid}$) and the growth integral (area under the curve, AUC). For the supernatant assays, we summed up all growth effects a species has on the other species and scaled them across species. To scale relative fitness values in co-culture assays, we implemented a stepwise process to avoid double-counting of the reciprocal fitness value. We started with the weakest species and summed up all its relative fitness values. Then we moved to the second (third) weakest species and repeated the procedure leaving out any fitness effects that were already accounted for before. For all experiments, we scaled the values from weakest (left) to strongest (right) performer. A line demarks the transition from neutral/positive to negative effects on the other species. (B) Species rank order from *in vivo* competition experiments in the larvae of *G. mellonella* 12 hours post infection from a previous study (19). The calculation of the species rank order was done as for the co-culture assays.

Can within-host species interactions be predicted from *in vitro* experiments?

Competitive metrics obtained from *in vitro* experiments are often taken as proxies to predict the competitive strength of species in polymicrobial infections. For example, *P. aeruginosa* typically outcompetes *Staphylococcus aureus in vitro* (27–29). Such results are then put forward to explain the prevalence of *P. aeruginosa* in co-infections with *S. aureus*. Here, we ask whether a direct translation of *in vitro* results to the host context is warranted. This is possible because we used the same four pathogens as in the co-infection experiments in *G. mellonella* insect larvae (19). The data from the previous in-host competition experiments are recapitulated in Fig. S5.

For the comparison, we take the *in vitro* results from GIM medium, which mimics the nutritional conditions of the insect environment. We find a moderate match between the rank orders observed in the *in vivo* and *in vitro* insect environment (Fig. 4). While K and P were among the stronger competitors in both environments, the

weakest agreements were observed for C and B. In GIM, C performed well whereas it was the poorest competitor in the *G. mellonella* host, not even able to grow within the observed 12 hours post infection period. Conversely, B was the weakest competitor in GIM, yet was competitive against both C and K in the host. This comparison suggests that host-pathogen interactions matter, highlighting that *in vitro* assays might not always be adequate predictors of *in vivo* dynamics.

Simulating higher-order interactions

Next, we used computer simulations based on our experimental monoculture growth and supernatant assay data to test whether simulated 3- and 4-species community interactions are predictive of the competitive rank order inferred from our pairwise co-culture experiments. A good match can be expected when pairwise effects are additive in larger communities.

A detailed description of our agent-based modeling platform is provided elsewhere (23). In brief, bacteria are modeled as disks growing on a two-dimensional continuous toroidal surface without boundaries. The growth and division of bacterial agents is determined by (i) the intrinsic growth parameter *g* and (ii) the (negative or positive) effects of secreted molecules taken up by the agent (see methods). We used the experimental data from GIM to parameterize (i) and (ii). For (i), we set *g* to a value between 0.5 and 1, scaled relative to the respective species rank order values shown in Fig. 4A for $1/T_{mid}$. For (ii), we also informed ourselves on the $1/T_{mid}$ data (Fig. 2) and modeled toxins that reduced the growth at least by 20% (Fig. 2). Accordingly, we had two toxins in the system (toxin by K inhibiting all other species, and toxin by B inhibiting P). Toxins are modeled as agents and are produced with a constant probability of 0.5 (per cell and time step) and diffuse according to a specified diffusion rate. Toxins are taken up by sensitive cells when the molecule and the bacterial agent physically overlap, and a toxin potency parameter defines how dramatically the growth of the target cell is reduced and how many toxins provoke death.

In a first set of simulations, we varied toxin potency (a parameter we could not estimate empirically) to recover the results from our pairwise co-culture experiments. We found that a high toxin potency is required for K to beat C, while moderate toxin potencies suffice for K to beat P and B, and for P to withstand the attacks of B (Fig. S1). We thus implemented two toxin potencies in our models (strong toxin: 1,750 for K vs. C; weak toxin: 2,500 for the other three interactions).

For the main simulation, the 4-species community, we seeded all four species (32 founding agents per species) randomly to our landscape and let them grow for 30,000 time steps, growing and producing toxins according to the parameters inferred from our experiments. We simulated two scenarios, a high diffusion environment in which bacterial agents and toxins move readily (mimicking shaken liquid conditions), and a low diffusion environment in which bacterial agents do not move and toxins diffuse slowly (mimicking conditions where cells grow on surfaces). We ran chemostat-type simulations, where population size was kept constant at half carrying capacity (~ 500 cells). Our simulations revealed competitive rank orders for the low diffusion (B < P = K < C) and high diffusion (B < P < K < C) environments (Fig. 5A) that differ from the predicted rank order (B < P < C < K) based on our experimental co-culture results (Fig. 4A). Notably, C and K swapped places, indicating that the K toxin that was so potent to suppress C in pairwise competitions showed reduced efficacy in the 4-species community. How can this non-additive effect be explained? When looking at the toxin uptake rate, we observed that the slow-growing species B and P had the highest per capita toxin uptake rate (Fig. 5A). In other words, B and P seem to detoxify

the environment for the fast-growing C. Inglis et al. (30) described a similar phenomenon, however, in their study the toxin-producing cells removed a fraction of their own toxins from the environment by receptor-based translocation and neutralization inside the cell. They call this the toxin '(self-)soaking' effect. In our case, the toxin burden is distributed across all species except the producer, which could be described as a toxin 'absorption' effect. The fast-growing C benefits the most because it can dilute the per cell toxin concentration to below the killing threshold due to its fast replication in contrast to slow growers.

This raises the question whether the toxin absorption effect also manifests in 3-species communities (Fig. 5B-E). We found that a single slow-growing species (either P or B) is enough to create the toxin absorption effect so that the best performing species K in pairwise co-culture experiments is outpaced by C in multispecies communities (Fig. 5B+C). We then asked whether this toxin absorption effect can be circumvented by higher toxin potency. Indeed, we found this to be the case, but only when K's toxin was extremely potent and only under high diffusion conditions (Fig. S6). Importantly, the toxin absorption effect against K's toxin did not occur in the B+K+P community, where K is the fastest growing species (Fig. 5D). In this community, spatial structure had an important effect by greatly reducing toxin uptake rates and allowing species to coexist. Altogether, our simulations reveal that the toxin absorption effect and spatial structure attenuate toxin effects in multispecies communities.

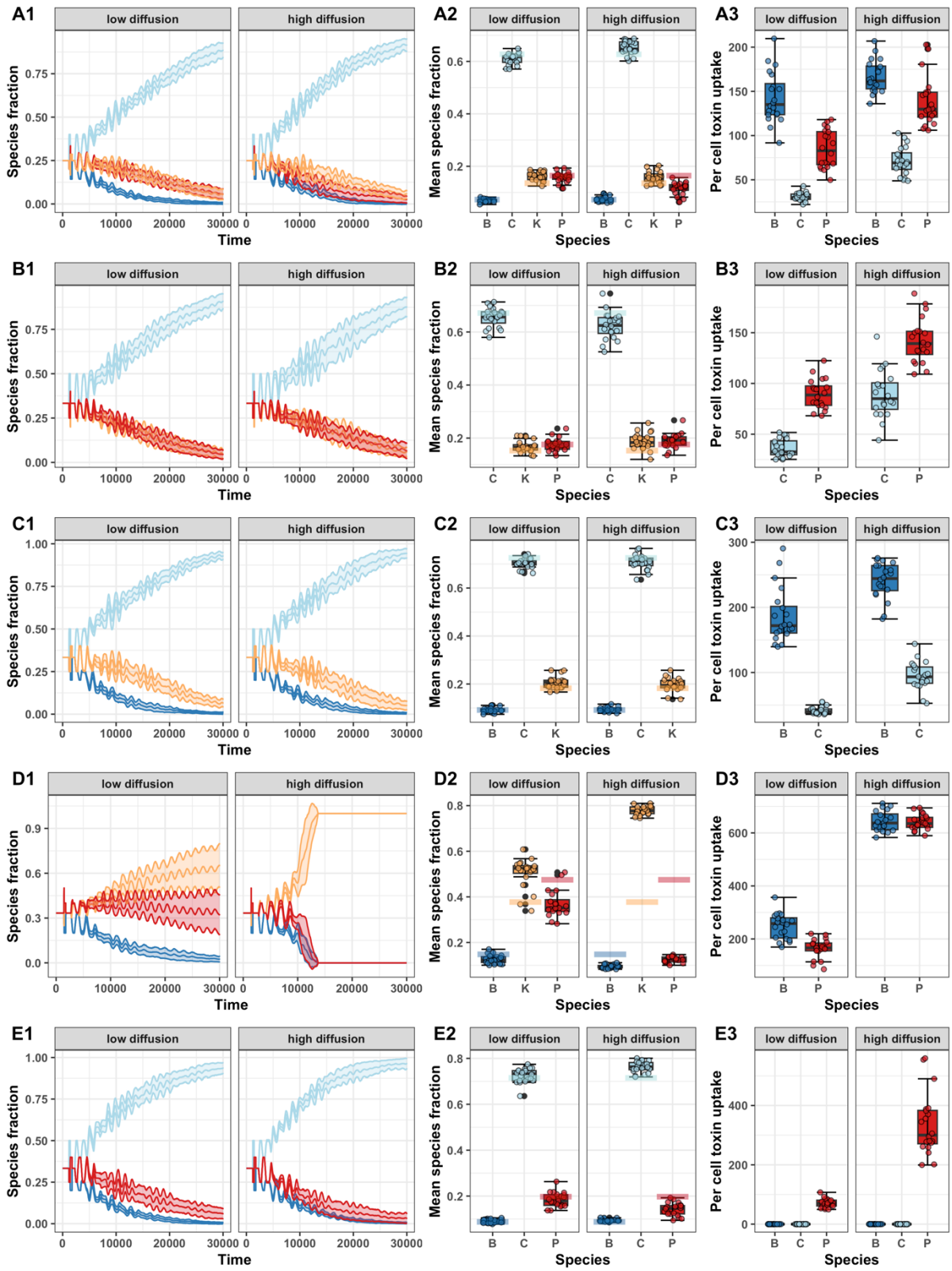

Figure 5. Bacterial community dynamics simulated with an agent-based model and parameterised with experimental growth and inhibition data. Panels show the (1) species fractions over time, (2) mean species fraction over time, (3) per cell toxin uptake for (A) the 4-species community and (B-E) all combinations of 3-species communities. All simulations were carried out under low diffusion (cell diffusion D = 0.0 μm^2 s^{-1}, toxin diffusion ∂ = 0.1 μm^2 s^{-1}, a structured environment) and high diffusion (cell diffusion D = 5.0 μm^2 s^{-1}, toxin diffusion ∂ = 10.0 μm^2 s^{-1}, an unstructured environment). In (1), lines show the mean and the standard

deviation across 20 independent simulations. Boxplots show the median values (line within the box) across the 20 simulations with the first and third quartiles. The whiskers cover 1.5x of the interquartile range or extend from the lowest to the highest value if all values fall within the 1.5x interquartile range. In (2), the shaded boxes depict the simulated mean species fraction in the absence of toxins.

Discussion

Bottom-up experimental approaches, in which a small number of bacterial species are mixed, have become popular to derive principles of community dynamics and stability (3–9). Although co-culture experiments directly reveal winners and losers, they are often challenging to conduct. Specifically, co-culture experiments require measuring species frequencies, which rely on phenotypic (morphological) or genotypic (fluorescence, antibiotic, etc.) markers to distinguish the species. However, counting colonies is labor-intensive and markers are often hard to introduce and limited in numbers. To overcome these limitations, we asked whether pairwise interaction outcomes and the resulting species rank order can be inferred from monoculture growth and supernatant assays without the need of mixing species. While monoculture growth assays provide information on how well a species grows in a particular medium, supernatant assays provide information on secreted compounds that have inhibitory or stimulatory effects on opponents. Using a 4-species community, we found that pairwise competition outcomes can be predicted to a large extent based on these two assays. In particular, we observed that monoculture growth is the most important factor predicting competition outcomes and supernatant effects allow fine-tuning of the species' competitive rank order. We further used an agent-based model, parameterised with our empirical data, to show that dynamics in multispecies communities match well the species rank order derived from monoculture and supernatant data with one important exception. The effect of inhibitory compounds is attenuated in multispecies communities, leading to an even higher predictive power of monoculture growth parameters.

Our procedure is based on three simple rules to predict species competitive ranks from monoculture growth and supernatant assays. It starts with the ranking of the species according to their monoculture growth performance (rule 1). Subsequently, species showing intermediate growth yet produce inhibitory compounds for other species are moved further up in the ranking (rule 2), while inhibitory effects by slow-growing species are ignored (rule 3). The last rule applies because inhibitory compounds of slow-growing species do not reach a high enough concentration to be effective in co-culture. The use of such simple rules comes with several advantages. First, the experimental data the rules are based on are easy to collect. This saves both effort and resources. Growth curve and supernatant experiments solely rely on measuring OD. They do not require labor-intensive pairwise co-culture experiments in which individual species must be adjusted to the same frequency, mixed, plated, and colonies counted based on unambiguous markers (e.g., phenotypic, fluorescence, antibiotic markers) (10,31–34). Second, the simplicity of the methods allows to scale up experiments, involving more and larger communities to be analyzed in parallel.

A key next step is to assess the generality of the rules. We used two different growth media to derive our rules. For GIM, the rules worked well. For LB, we found that a good match between predicted and observed competitive ranks depended on the growth parameters used. Our results suggest that more integrative growth parameters ($1/T_{mid}$ and AUC) work better than maximal growth rate to predict

competition outcomes. While growth rate or maximum culture density (yield) are most commonly used as fitness parameters (35,36), our findings are in line with other studies, showing that single growth parameters cannot adequately capture overall fitness across the duration of an experiment (10,33,37). Our recommendation to use more integrative growth parameters clearly needs further validation. Overall, our rules need to be verified using different media, covering the range from nutrient-poor to nutrient-rich, as well as different environments, ranging from liquid to structured environments (i.e., on agar/agarose patches or in viscous liquid medium (13,29,38). In addition, our approach needs to be probed with other bacterial communities, both synthetic and natural bacterial assemblies with a higher number of species.

Our results show that monoculture growth and supernatant assay data can be combined to predict pairwise species interactions and to establish a species rank order at the community level. But how predictive is this species rank order for the species dynamics when all four species grow together? Our agent-based model revealed that the predictive power is considerably high, suggesting that effects observed in pairwise interactions are mostly additive in larger communities. However, there was one major exception. K was predicted to be the most competitive species based on the empirical data, whereas the computer simulations yielded C as the clear winner. This discrepancy can be explained by what we call the 'absorption effect' in multispecies compared to pairwise interactions: K produces an inhibitory compound (detected in the supernatant assay and modeled as a toxin), for which slower growing community members (B and P) have the highest per capita toxin uptake rates. Thereby, they detoxify the environment for the fastest growing species (C). This non-additive effect indicates that the potency of toxins (derived from supernatant data) might be overestimated in multispecies communities. Thus, our simulation results affect the relative impact of our rules: it increases the weight of monoculture growth performance (rule 1) relative to supernatant effects (rule 2) in predicting competitive strengths in multispecies communities. Overall, we show that agent-based models can efficiently complement experimental data in several ways. First, higher-order interactions in multispecies communities can be examined that are difficult to test experimentally. Second, long-term species dynamics can be tracked. Finally, non-additive mechanisms such as the toxin absorption effect can be detected (39).

Another important finding of our work is that species competitive rank orders differ substantially across nutritional conditions. For example, P had a low competitive rank in GIM (3rd place), performed well in LB (2nd place) and was the top competitor in the larvae of *G. mellonella* (Figure 4). Our findings are in line with previous studies showing that change in nutritional conditions can alter species interactions from positive to negative relationships (3,4,40). Our results further suggest that special care must be taken when *in vitro* interaction data are used to forecast bacterial species interactions in infections.

In conclusion, our work reveals that the combination of monoculture growth parameters, strong inhibitory effects from supernatant assays and computer simulations is a powerful toolkit to predict pairwise and multispecies interaction outcomes in bacterial communities. Our approach now requires in-depth testing across a diverse set of environmental conditions and across different and more diverse bacterial communities. Moreover, in-detail investigations on the actual compounds causing growth inhibition in the supernatant assays (e.g., toxins, siderophores, biosurfactants, amino acids, or molecules affecting environmental conditions such as pH) could further help to fine-tune predictions of competition outcomes.

Data availability
All raw data sets will be deposited in the figshare repository.

Supplementary information
Supplementary information will be made available online.

Acknowledgements
We thank Richard Allen for his help with the statistics of this study. We also thank Alex Hall, Kayla King, Anna-Liisa Laine, and Roland Regoes for their scientific input.

Funding
This project has received funding from the Swiss National Science Foundation (grant no. 31003A_182499 to RK).

Compliance with ethical standards
Conflict of interest: The authors declare that they have no conflict of interest.

Bibliography
1. Widder S, Allen RJ, Pfeiffer T, Curtis TP, Wiuf C, Sloan WT, et al. Challenges in microbial ecology: Building predictive understanding of community function and dynamics. Vol. 10, ISME Journal. 2016.
2. Louca S, Jacques SMS, Pires APF, Leal JS, Srivastava DS, Parfrey LW, et al. High taxonomic variability despite stable functional structure across microbial communities. Nat Ecol Evol. 2016 Dec 5;1(1).
3. Piccardi P, Vessman B, Mitri S. Toxicity drives facilitation between 4 bacterial species. Proc Natl Acad Sci U S A. 2019;116(32):15979–15984.
4. Ratzke C, Barrere J, Gore J. Strength of species interactions determines biodiversity and stability in microbial communities. Nat Ecol Evol [Internet]. 2020;4(3):376–83. Available from: http://dx.doi.org/10.1038/s41559-020-1099-4
5. Preussger D, Giri S, Muhsal LK, Oña L, Kost C. Reciprocal Fitness Feedbacks Promote the Evolution of Mutualistic Cooperation. Current Biology. 2020;30(18):3580-3590.e7.
6. Sundarraman D, Hay EA, Martins DM, Pettinari NL, Parthasarathy R, Drew S. Quantifying multi-species microbial interactions in the larval zebrafish gut. 2020;1–23.
7. Pontrelli S, Szabo R, Pollak S, Schwartzman J, Ledezma-Tejeida D, Cordero OX, et al. Metabolic cross-feeding structures the assembly of polysaccharide degrading communities. Sci Adv. 2022;8(8):1–12.
8. Figueiredo ART, Özkaya Ö, Kümmerli R, Kramer J. Siderophores drive invasion dynamics in bacterial communities through their dual role as public good versus public bad. Ecol Lett. 2022;25(1):138–50.
9. Diaz-Colunga J, Lu N, Sanchez-Gorostiaga A, Chang CY, Cai HS, Goldford JE, et al. Top-down and bottom-up cohesiveness in microbial community coalescence. Proc Natl Acad Sci U S A. 2022 Feb 8;119(6).
10. Concepción-Acevedo J, Weiss HN, Chaudhry WN, Levin BR. Malthusian parameters as estimators of the fitness of microbes: A cautionary tale about the low side of high throughput. PLoS One. 2015 Jun 26;10(6).
11. Nestor E, Toledano G, Friedman J. Interactions between Culturable Bacteria Are Predicted by Individual Species' Growth. mSystems. 2023 Apr 27;
12. Ghoul M, Mitri S. The Ecology and Evolution of Microbial Competition. Trends Microbiol [Internet]. 2016;24(10):833–45. Available from: http://dx.doi.org/10.1016/j.tim.2016.06.011
13. Chao L, Levin BR. Structured habitats and the evolution of anticompetitor toxins in bacteria. Proceedings of the National Academy of Sciences USA [Internet]. 1981;78(10):6324–8. Available from: https://www.pnas.org
14. Pinu FR, Granucci N, Daniell J, Han TL, Carneiro S, Rocha I, et al. Metabolite secretion in microorganisms: the theory of metabolic overflow put to the test. Vol. 14, Metabolomics. Springer New York LLC; 2018.

15. Enke TN, Datta MS, Schwartzman J, Cermak N, Schmitz D, Barrere J, et al. Modular Assembly of Polysaccharide-Degrading Marine Microbial Communities. Current Biology. 2019;29(9):1528–35.
16. Aoki SK, Pamma R, Hernday AD, Bickham JE, Braaten BA, Low DA. Contact-Dependent Inhibition of Growth in Escherichia coli. Science (1979). 2005 Apr 2;309:1245–8.
17. Danka ES, Garcia EC, Cotter PA. Are CDI Systems Multicolored, Facultative, Helping Greenbeards? Vol. 25, Trends in Microbiology. Elsevier Ltd; 2017. p. 391–401.
18. Coulthurst S. The Type VI secretion system: A versatile bacterial weapon. Microbiology (United Kingdom). 2019 May 1;165(5):503–15.
19. Schmitz DA, Allen RC, Kümmerli R. Negative interactions and virulence differences drive the dynamics in multispecies bacterial infections. Proceedings of the Royal Society B (*in press*).
20. Harding CR, Schroeder GN, Collins JW, Frankel G. Use of Galleria mellonella as a model organism to study Legionella pneumophila infection. Journal of Visualized Experiments. 2013;81:1–10.
21. Andrea A, Krogfelt KA, Jenssen H. Methods and challenges of using the greater wax moth (Galleria mellonella) as a model organism in antimicrobial compound discovery. Microorganisms. 2019;7(3):1–9.
22. Wojda I, Staniec B, Sułek M, Kordaczuk J. The greater wax moth Galleria mellonella: Biology and use in immune studies. Pathog Dis. 2020;78(9):1–15.
23. Wechsler T, Kümmerli R, Dobay A. Understanding policing as a mechanism of cheater control in cooperating bacteria. J Evol Biol. 2019;32(5):412–24.
24. Dobay A, Bagheri HC, Messina A, Kümmerli R, Rankin DJ. Interaction effects of cell diffusion, cell density and public goods properties on the evolution of cooperation in digital microbes. J Evol Biol. 2014;27(9):1869–77.
25. Stover CK, Pham XQ, Erwin AL, Mizoguchi SD, Warrener P, Hickey MJ, et al. Complete genome sequence of Pseudomonas aeruginosa PAO1, an opportunistic pathogen. Nature. 2000;406(6799):959–64.
26. Mahenthiralingam E, Coenye T, Chung JW, Speert DP, Govan JRW, Taylor P, et al. Diagnostically and experimentally useful panel of strains from the Burkholderia cepacia complex. J Clin Microbiol. 2000;38(2):910–3.
27. Mashburn LM, Jett AM, Akins DR, Whiteley M. Staphylococcus aureus serves as an iron source for Pseudomonas aeruginosa during in vivo coculture. J Bacteriol. 2005 Jan;187(2):554–66.
28. Filkins LM, Graber JA, Olson DG, Dolben EL, Lynd LR, Bhuju S, et al. Coculture of Staphylococcus aureus with Pseudomonas aeruginosa drives S. aureus towards fermentative metabolism and reduced viability in a cystic fibrosis model. J Bacteriol. 2015;197(14):2252–64.
29. Niggli S, Kümmerli R. Strain Background, Species Frequency, and Environmental Conditions Are Important in Determining Pseudomonas aeruginosa and Staphylococcus aureus Population Dynamics and Species Coexistence. Appl Environ Microbiol. 2020;86(18):1–14.
30. Inglis RF, Hall AR, Buckling A. The role of “soaking” in spiteful toxin production in Pseudomonas aeruginosa. Biol Lett. 2013 Feb 23;9(1).
31. Gallet R, Cooper TF, Elena SF, Lenormand T. Measuring selection coefficients below 10-3: Method, Questions, and Prospects. Genetics. 2012;190(1):175–86.
32. Wiser MJ, Lenski RE. A comparison of methods to measure fitness in Escherichia coli. PLoS One. 2015 May 11;10(5).
33. Ram Y, Dellus-Gur E, Bibi M, Karkare K, Obolski U, Feldman MW, et al. Predicting microbial growth in a mixed culture from growth curve data. 2019;116:14698–707.
34. Hegreness M, Shoresh N, Hartl D, Kishony R. An Equivalence Principle for the Incorporation of Favorable Mutations in Asexual Populations. Science (1979). 2006 Mar 17;311(5767):1615–7.
35. Adamberg K, Kask S, Laht TM, Paalme T. The effect of temperature and pH on the growth of lactic acid bacteria: A pH-auxostat study. Int J Food Microbiol. 2003 Aug 15;85(1–2):171–83.

36. Hall BG, Acar H, Nandipati A, Barlow M. Growth rates made easy. Mol Biol Evol. 2014 Jan;31(1):232–8.
37. Li Y, Venkataram S, Agarwala A, Dunn B, Petrov DA, Sherlock G, et al. Hidden Complexity of Yeast Adaptation under Simple Evolutionary Conditions. Current Biology. 2018 Feb 19;28(4):515-525.e6.
38. Granato ET. Low spatial structure and selection against secreted virulence factors attenuates pathogenicity in Pseudomonas aeruginosa. ISME J [Internet]. 2018; Available from: http://dx.doi.org/10.1038/s41396-018-0231-9
39. Lopatkin AJ, Collins JJ. Predictive biology: modelling, understanding and harnessing microbial complexity. Nat Rev Microbiol [Internet]. Available from: http://dx.doi.org/10.1038/s41579-020-0372-5
40. Kehe J, Ortiz A, Kulesa A, Gore J, Blainey PC, Friedman J. Positive interactions are common among culturable bacteria [Internet]. Vol. 7, Sci. Adv. 2021. Available from: https://www.science.org